ELSEVIER

Journal of Photochemistry and Photobiology A: Chemistry 98 (1996) 65–72

Journal of PHOTOCHEMISTRY AND PHOTOBIOLOGY A: CHEMISTRY

Spectroscopic and photophysical properties of some new rhodamine derivatives in cationic, anionic and neutral micelles

P. Pal [a], H. Zeng [a], G. Durocher [a,*], D. Girard [b], R. Giasson [b,*], L. Blanchard [c], L. Gaboury [c], L. Villeneuve [c,*]

[a] *Laboratoire de photophysique moléculaire, Département de chimie, Université de Montréal, C.P. 6128, Succ. Centre-ville, Montréal, Qué., H3C 3J7, Canada*

[b] *Laboratoire de photochimie organique, Département de chimie, Université de Montréal, C.P. 6128, Succ. Centre-ville, Montréal, Qué., H3C 3J7, Canada*

[c] *Laboratoire de pathologie moléculaire, Département de Pathologie, Université de Montréal, C.P. 6128, Succ. Centre-ville, Montréal, Qué., H3C 3J7, Canada*

Abstract

The spectroscopic and photophysical characterization of rhodamine 123 (dye **1**), 4,5-dibromorhodamine methyl ester (dye **2**) and 4,5-dibromorhodamine n-butyl ester (dye **3**) are reported in homogeneous media like water and some alcohols and also in microheterogeneous media; anionic sodium dodecylsulfate (SDS), cationic cetyltrimethylammonium bromide (CTAB) and neutral triton X-100 (TX) micelles. The selective biodistribution of these ionic drugs in tissues and membranes strongly influence their photosensitizing properties which have been part of our earlier studies. Results suggest that the hydrogen bonding capability of the amino end group lone pair of these dyes dominates in water. All these dyes interact with anionic SDS micelles. The interaction is mainly electrostatic in nature. At low SDS concentrations (below c.m.c.), dye–SDS aggregate formation takes place. But above c.m.c. only the monomeric dye form is observed. The penetration of dye **3** in SDS is a little less compared to dyes **1** and **2**. Dyes **2** and **3** show a finite interaction with CTAB micelle unlike dye **1**. With neutral TX micelles all the dyes form strong complexes. The fluorescence quantum yield (Φ_F) of these three dyes in TX is lower. In time-resolved fluorescence experiments, two lifetimes are observed. The effects of the TX concentration on the fluorescence decay are measured. The decay associated spectra of dye **2** in TX are obtained by global compartmental analysis. The dye-surfactant interaction mechanisms are also discussed.

Keywords: Rhodamine dye; Spectroscopic properties; Photophysical properties

1. Introduction

Photodynamic therapy (PDT), which defines the use of photosensitizing chemicals combined with light to produce singlet oxygen, is a modality for cancer treatment [1]. Recently, we have synthesized some bromine substituted cationic rhodamine dyes namely, 4,5-dibromorhodamine methyl ester (dye **2**) and 4,5-dibromorhodamine n-butyl ester (dye **3**) (Fig. 1). Our earlier work [2] shows that these newly synthesized dyes are very good singlet oxygen producers and could be used as efficient cancer cell photosensitisers for potential uses in in vitro bone marrow purging in the preparation of autologous bone marrow transplantation.

The extent of the photodynamic action depends not only on the singlet oxygen production but also on the biodistribution of the ionic dye in the cytoplasmic and mitochondrial membranes, the retention and the nature of the binding inside the cell. The binding sites and the microenvironment sur-

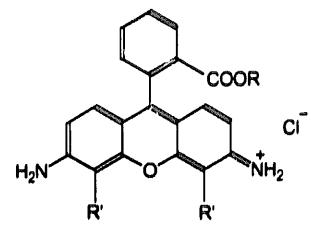

Dye 1	R = CH_3	R' = H	Rhodamine 123
Dye 2	R = CH_3	R' = Br	4,5-Dibromo rhodamine methyl ester
Dye 3	R = $(CH_2)_3CH_3$	R' = Br	4,5-Dibromo rhodamine n-butyl ester

Fig. 1. Molecular structures of dyes **1**, **2** and **3**.

* Corresponding authors.

PII S1010-6030(96)04351-1

rounding dye molecules inside the cell are indeed complex in nature and influence the photophysical properties of the dye. As micellar media are considered simple membrane mimetic systems [3], over the past few decades, there has been a widespread interest in studying the spectroscopic and photophysical properties of photosensitizing dyes in micellar media for a better understanding of the nature of localization and interaction in a true biological systems.

Recently, the spectroscopic characterization of rhodamine 123 in SDS and in CTAB micellar media has been reported [4]. Only one detailed steady state and time resolved spectroscopic study has been performed in neutral TX micelles [5]. But rhodamine dyes in TX have nevertheless been considered as a model system to compare the microenvironment of the dye facing inside the biological systems [6]. In order to obtain a better understanding of the nature of the interaction of these new dyes in the biological systems, studies of the spectral characteristics of these dyes in the presence of surfactants are essential. Among the various techniques employed, fluorescence has turned out to be one of the most powerful techniques due to its excellent sensitivity and its time domain [7,8]. Time-resolved spectroscopy is the ideal technique to unravel the often complex kinetics of the excited-state processes. In recent articles [9,10] we have used various models to analyze fluorescence decay traces. The measurement of the multidimensional fluorescence decay surface as a function of various experimental conditions provides data with a high accuracy allowing for elaborate data analysis [11]. The analysis of all related experimental fluorescence decay traces in a single step is the most appropriate way to discriminate between the competing kinetic models and to obtain the most reliable parameter estimated. In the so-called global analysis approach [12], the parameters can be linked over various decay traces. The power and performance of this method have been extensively demonstrated [13].

In this article, we report on the steady state spectral and the photophysical properties of these newly synthesized dyes together with dye 1 in homogeneous media: water, methanol, ethanol, n-butanol, n-hexanol and also in heterogeneous media: sodium dodecylsulfate (SDS), cetyltrimethylammonium bromide (CTAB) and triton X-100 (TX) micelles. The dye–surfactant interaction mechanism is discussed. Special attention is put on the dye–TX complex. We use the single-photon counting technique to obtain the fluorescence decay traces. The TX concentration and the emission-wavelength dependence of the fluorescence decay of dye 2 in TX are analyzed globally to get more insight into the nature of the complexation.

2. Experimental details

Rhodamine 123 (Aldrich) and rhodamine B (Eastman Kodak) were used as received after checking the purity by HPLC. Dyes 2 and 3 were synthesized in our laboratory. Details of the synthesis and purification are described elsewhere [2]. The purity of the synthesized dyes is greater than 99%. Spectrophotometric grade solvents were used as received. The surfactants, SDS, (Aldrich, 98%) and CTAB (Aldrich, 95%) were used after being purified according to the method reported recently [14]. TX (Fluka, 99%) was used as received. Doubly distilled deionized water was used as a solvent. The pH of the water and of the micellar media is maintained at about 6.3. All these dyes are in esterified form and no pH effect was observed within the range 1–12 [15].

The absorption spectra were recorded on a Philips PU-8800 UV–vis spectrophotometer. The corrected fluorescence spectra were recorded on a Spex Fluorolog-2 spectrofluorometer with a F2T11 special configuration. The fluorescence lifetimes were measured on a multiplexed time-correlated single-photon counting fluorometer (Edinburgh Instruments, Model 299T). Details of the instrumental setup are already described elsewhere [16]. For spectroscopic measurements, the dye concentration was always kept below 2×10^{-6} M in order to avoid dye aggregation and reabsorption effects. To avoid any aggregation we checked that the Beer–Lambert law is valid in the concentration range we have studied. Freshly prepared solutions were always used. Fluorescence quantum yields were measured using zwitterionic rhodamine B in methanol ($\Phi_F=0.53$) as a standard [17]. All measurements were carried out at room temperature (25 °C).

The analysis of the entire decay including the rising edge was performed by the deconvolution method. The goodness of the fit has been assessed from the statistical parameters χ^2 and DW (Durbin–Watson) [16]. Lifetime data were also analyzed by the global analysis method assuming that the fluorescence decay can be represented as a sum of the exponential components:

$$I(t)=\sum_i \alpha_i \exp(-t/\tau_i) \quad (1)$$

where, τ_i and α_i are the lifetime and the pre-exponential factor of the ith component respectively. A global iterative reweighted reconvolution program based on a nonlinear least-squares method was used (Global unlimited, Urbana, IL) [18]. The lifetime data were both individually and globally analyzed by using single, double or triple exponentials. To obtain the influence of the TX concentration on the fluorescence lifetime and to recover the decay-associated spectra (DAS), decays were measured at different TX concentrations and at different emission wavelengths respectively and were analyzed globally by linking the lifetime and allowing the αs to float independently. The pre-exponential factors were normalized and the fractional fluorescence intensity was calculated as

$$I_i=\alpha_i\tau_i/\sum_i \alpha_i\tau_i \quad (2)$$

The wavelength dependence of each fraction produces the DAS of the corresponding species. The sum of these fractions

Table 1
Spectroscopic and photophysical data of the rhodamine dyes in water, alcohols and micellar media

Samples	Solvents	Abs. max (nm)	$FWHM_{abs.}$ (cm^{-1})	Em. max (nm)	$FWHM_{em.}$ (cm^{-1})	Stokes shift (cm^{-1})	ϕ_F	τ_F* (ns)	$k_F \times 10^{-8}$ (s^{-1})	$k_{nr} \times 10^{-7}$ (s^{-1})
Dye 1	Water	498	1400	525	1600	1050	0.87	4.2	2.1	3.1
	Methanol	503	1160	527	1450	920	0.86	4.2	2.1	3.3
	Ethanol	507	1180	530	1360	870	0.86	4.0	2.2	3.5
	n-Butanol	512		533		790	0.90	3.9	2.3	4.3
	n-Hexanol	513		534		770	0.95			
	SDS (0.05M)	507	1260	532		920	0.83	4.6	1.8	3.6
	CTAB (0.017M)	498		525	1490	1030	0.91	3.9	2.3	2.3
	TX (0.017M)	510		535		920	0.62 [a]	3.6	1.7	11
Dye 2	Water	504	1420	531	1500	1010	0.34	1.6	2.1	40
	Methanol	510	1200	536	1340	930	0.56	2.4	2.3	18
	Ethanol	513	1230	538	1110	920	0.52	2.5	2.1	20
	n-Butanol	516		539		850	0.52	2.5	2.1	19
	n-Hexanol	518		542			0.51			
	SDS (0.05M)	512	1370	538	1420	960	0.35	2.1	1.7	31
	CTAB (0.017M)	506		534		1050	0.26	1.6	1.6	46
	TX (0.017M)	515		542		970	0.14 [a]	1.3	1.1	67
Dye 3	Water	505	1350	531	1400	970	0.32	1.6	2.0	43
	Methanol	510	1200	535	1300	910	0.48	2.4	2.0	22
	Ethanol	514	1190	538	1200	870	0.47	2.4	2.0	22
	n-Butanol	518		539		770	0.48	2.6	1.9	20
	n-Hexanol	520		542			0.49			
	SDS (0.05M)	509	1340	535	1430	950	0.39	2.0	1.9	30
	CTAB (0.017M)	511		537		950	0.22	1.6	1.4	49
	TX (0.017M)	516		540		860	0.13 [a]	1.2	1.1	70

FWHM = Full width at half maximum.
ϕ_F = Fluorescence quantum yield.
τ_F = Fluorescence lifetime.
k_F = Radiative rate constant = ϕ_F / τ_F.
k_{nr} = Non radiative rate constant = $(1 - \phi_F)/\tau_F$.
* = Lifetime values presented are obtained from single exponential decay except those in TX. in TX values are mean life time $\langle \tau \rangle$ as defined in the experimental section.
[a] The fluorescence quantum yield corresponds to the sum of yields of free and complexed dye.

at a particular wavelength should be proportional to the steady-state intensity measured at the corresponding wavelength. We have also calculated the average lifetime $\langle \tau \rangle$ using the formula for the second moment

$$\langle \tau \rangle = \sum_i \alpha_i \tau_i^2 / \sum_i \alpha_i \tau_i \quad (3)$$

3. Results and discussion

We have measured the absorption spectra, emission spectra, fluorescence quantum yields and the lifetimes for these dyes in homogeneous solvents like water, different alcohols and in microheterogeneous micellar media like anionic SDS, cationic CTAB and neutral TX. The results are shown in Table 1. The micellar concentrations are kept above the critical micellar concentration (c.m.c.) for all the micellar results presented in this table. In SDS and TX we have also studied the micellar concentration dependence of the spectroscopic and the photophysical properties of these dyes. Results are presented and discussed categorically in the following subsections.

3.1. In homogeneous media

From Table 1, one can see that owing to bromination, the absorption and emission maxima are slightly red-shifted. It is observed that for the three dyes, the absorption and emission maxima are shifted to the blue with a concomitant general broadening of the bands going from alcohols to water. This result is opposite to a normal solvatochromic effect where the excited state is more stabilized in a more polar solvent giving rise to red-shifted absorption and emission bands. This result shows the hydrogen-bonding capability of the amino end group of the dyes, which increases with the increasing proton donor ability of protic solvents. This is a well-known phenomenon occurring in aromatic amines, which is attributed to the hydrogen-bonding interaction (more important in water than in alcohols) involving the lone pair of the terminal nitrogen atom. This is called the "blue shift anomaly" observed in amino molecules dissolved in protic solvents [19–21]. The protic solvent acts as a hydrogen bond donor to the lone pair of the terminal amino group causing a reduced conjugation with the aromatic moiety. In some cases, this has the consequence of reducing the planarity

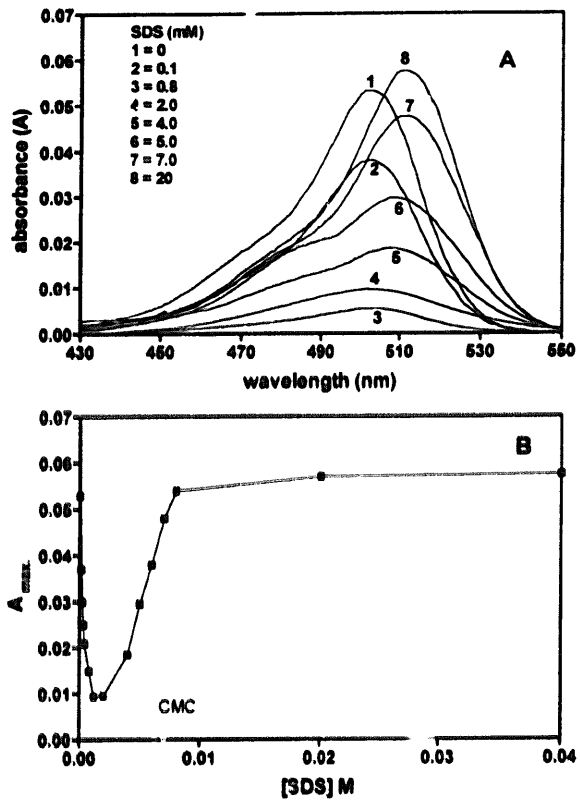

Fig. 2. (a) Room temperature (25 °C) absorption spectra of dye 2 in water and in SDS at different SDS concentrations. Concentration of dye 2 is 8.0×10^{-7} M in a 1 cm square cell. (b) SDS concentration dependence of the absorbance at absorption maxima of dye 2. The dotted line indicates the critical micellar concentration of SDS.

of the whole molecular skeleton in the ground and the relaxed excited state. Consequently, the absorption and fluorescence band broadened accordingly. Table 1 shows that this is indeed the case, the absorption and fluorescence bandwidths generally increase going from n-hexanol to water. Even though the change is rather small, it may help to elucidate the average site of these dyes in microheterogeneous micellar media.

In the case of dye 1, it is also observed that ϕ_F and τ_F and consequently, k_F and k_{nr} are almost independent of the solvent as far as the alcohols are concerned. But in dyes 2 and 3 there is a definite decrease in ϕ_F and τ_F from alcohols to water. As the k_F values are almost identical, this decrease suggests that in water non-radiative processes increase for dyes 2 and 3. Our earlier estimations [2] of the triplet quantum yield and singlet oxygen quantum yield of these dyes suggest that in water internal conversion due to the rotational relaxation of the amino group increases.

3.2. *In anionic SDS micelle*

We have studied the effect of anionic SDS micelles on the spectroscopic and photophysical properties of dyes 1, 2 and 3. Fig. 2(a) shows the absorption spectra of dye 2 at different SDS concentrations. Fig. 2(b) shows the change in absorbance at the absorption maxima with increasing [SDS]. With increasing [SDS] the absorbance decreases gradually (without any shift in the absorption maximum) to reach a minimum ([SDS]/[dye 2] = 1000) and then begins to grow up (with a red shift in the absorption maximum) to reach the maximum at [SDS] ≈ c.m.c. (the critical micellar concentration = 8×10^{-3} M [22]). Further increase in [SDS] above the c.m.c. does not influence the absorption spectrum. Similar changes are also observed in fluorescence. Dyes 1 and 3 also behave similarly in SDS micelles. Recently, similar observations with cationic rhodamine 123 in anionic SDS and in anionic D-L-α dipalmitoyl-phosphatidyl-L-serine (DPPS) vesicles were reported and discussed in details [4]. The decrease in the absorbance and emission intensity with increasing [SDS] (below c.m.c.) can be explained in terms of dye–surfactant aggregate formation. At very low [SDS], far below c.m.c., there is a formation of a dye–surfactant salt starting with the ion pair D^+S^- and continuing with dye–surfactant aggregates depicted as $(D^+S^-)_n$, all species being associated with lower fluorescence due to the average distance between the dye molecules in $(D^+S^-)_n$ which is greatly reduced and hence, facilitate self quenching [23]. Near and just below the c.m.c., the progress of the reorganization of $(D^+S^-)_n$ aggregates into premicelles with a monomeric D^+ content results in an increase in the absorbance and fluorescence intensity in this higher premicellar region (just below the c.m.c.) showing that the presence of premicelles provides the dye with the micellar-like environment. On a further increase of [SDS], the absorbance and fluorescence intensity reach the limiting value and all dye molecules are compartmentalized into normal micelles in monomeric form.

As far as the interaction of these dyes with anionic SDS micelles is concerned, all dyes interact almost identically. When the concentration of SDS is above the c.m.c., the absorption and emission maxima are red-shifted compared with those in water. The absorption and emission maxima indicate that dyes 1 and 2 are solubilized in SDS and are facing an ethanolic-like media. An increase in the fluorescence quantum yield and the lifetime also indicates that the dyes are protected against water in this environment. Dye 3 behave slightly differently. Here shifts are a little less. Its penetration inside the micelle might be hampered.

3.3. *In cationic CTAB micelle*

We have studied the effect of cationic CTAB (c.m.c. = 1×10^{-3} M [22]) micelles at the higher micellar concentration (0.017 M) on the spectroscopic and photophysical properties of dyes 1–3. For dye 1 small changes in absorption and emission spectra are observed compared to water (Table 1). The emission spectrum may be a little bit blue-shifted but this shift is within the limit of the instrumental sensitivity. ϕ_F and τ_F are almost unchanged. These results indicate that due to the repulsive electrostatic interaction dye 1 does not solubilize in CTAB micelle and remains in the water phase.

For dyes **2** and **3** distinct changes in the absorption and emission spectra are observed. Both are red-shifted compared with water. More important shifts are observed for dye **3**. The ϕ_F, τ_F and k_F values also decrease. These results indicate that dyes **2** and **3** are solubilized in CTAB micelles and that the extent of the penetration is higher with dye **3**. A small but distinct decrease in k_F indicates that there may be some weak complex formation for dyes **2** and **3**. At this stage it is difficult to understand why dyes **2** and **3** interact with CTAB when no interaction is perceived with dye **1**. But compared with dye **1**, dyes **2** and **3** contain two big bromine atoms and dye **3** contains a bulky n-butyl ester group. Thus, dyes **2** and **3** are more bulky and hydrophobic than dye **1**. It seems that there are two types of competitive interaction taking place. One is an electrostatic interaction and the other is a hydrophobic interaction. In dyes **2** and **3**, the hydrophobic interaction seems to dominate over the electrostatic repulsion and hence facilitates solubilization in CTAB micelles. Van der Waals'-surface-bounded molecular volume calculations, based on the grid calculation method [24] implemented in the HYPERCHEM software package [25,26] were obtained for these molecules and are shown in Table 2. We have also tabulated log *P* values which are the log of the octanol–water partition coefficient, a measure of hydrophobicity [27]. From these calculations it is quite clear that dyes **2** and **3** are much more hydrophobic than dye **1** as discussed above.

3.4. In neutral Triton X-100 micelles

Table 1 shows the spectroscopic and photophysical properties of the three dyes in TX at a micellar concentration above the c.m.c. (2×10^{-4} M [22]). In all of the dyes, large red shifts in the absorption and emission spectra are observed compared with water. Drastic changes in the fluorescence quantum yield and the lifetime are also observed. The results indicate that these dyes strongly interact with TX.

To elucidate the nature of the interaction, we have studied the TX concentration dependence on the spectroscopic and photophysical properties of the dyes. Fig. 3 shows the absorption spectra of mixed solutions with a fixed concentration of dye **2** and various concentrations of TX above the c.m.c. in an aqueous medium. The dye in water absorbs maximally at 504 nm. The spectrum shifts to 515 nm in the presence of TX with an isosbestic point at 509 nm. The isosbestic point indicates a complexation between two species. One may be the free dye and the other the surfactant molecule. Similar observations were also made for the other two dyes. Assuming a 1:1 complex, the equilibrium constant (K_c) and molar extinction coefficient (ϵ_c) of the complex can be determined by using the following modified form of the Benesi–Hildebrand equation [28]:

$$\frac{[S][D]l}{d_c-d_0}=\frac{[S]}{\epsilon_c-\epsilon_0}+\frac{1}{K_c(\epsilon_c-\epsilon_0)} \quad (4)$$

where $[D]$ and $[S]$ are the initial molar concentrations of the dye and the surfactant respectively; l is the optical path length of the solution, d_c and d_0 are the absorbances of the dye at the absorption maximum of the complex with and without surfactant respectively, and ϵ_c and ϵ_0 are the respective molar extinction coefficients of the complex and the dye at the absorption maximum of the complex. However, it is a prerequisite for the equation in the present form that the condition $[S] \gg [D]$ should hold and that the complex absorbs at a wavelength where the surfactant is completely transparent. The values of K_c and ϵ_c can be obtained from Eq. (4) by

Table 2
Molecular volume, log of the octanol–water partition coefficient (P), equilibrium constant (K_c) and spectrophotometric properties (isosbestic point (λ_{iso}) and molar extinction coefficient (ϵ_c) of the dye–TX complexes at 25 °C)

Dye	Molecular volume (Å^3)	log P	K_c (mole^{-1})	λ_{iso} (nm)	ϵ_c (M^{-1} cm^{-1})
Dye **1**	971	5.76	370	503	63700
Dye **2**	1071	7.34	660	509	62650
Dye **3**	1208	8.55	735	512	60750

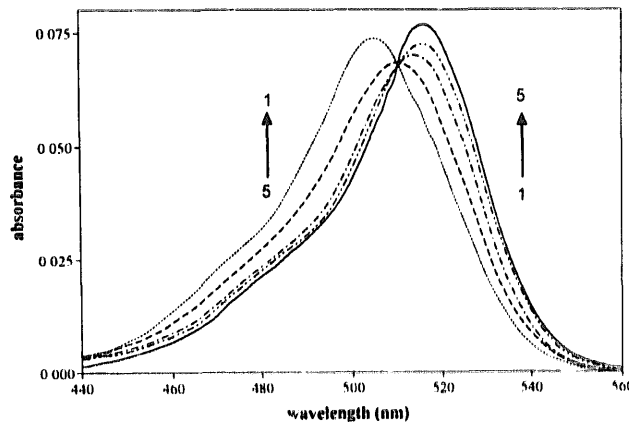

Fig. 3. Room temperature (25 °C) absorption spectra of dye **2** in water and in TX at different TX concentrations. Concentration of dye **2** is 1.54×10^{-6} M and concentrations of TX are (1) 0, (2) 1.09×10^{-3}, (3) 3.65×10^{-3}, (4) 9.12×10^{-3} and (5) 4.56×10^{-2} M.

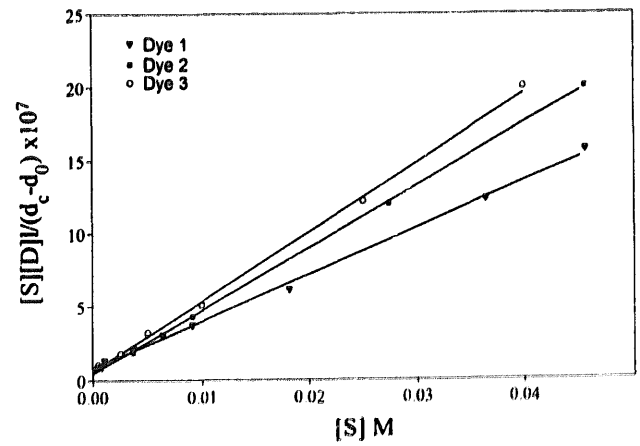

Fig. 4. $[S][D]l/(d_c-d_0)$ against $[S]$ plots for dyes **1**, **2** and **3** in TX micelle. The straight lines are obtained by linear least square fittings.

plotting $[S][D]l/(d_c-d_0)$ against $[S]$. Fig. 4 shows such plots for the three dyes. The plots are found to be linear in all cases confirming the 1:1 complex formation. From the slope and the intercept, K_c and ϵ_c can be calculated. Values are shown in Table 2, where it can be seen that the K_c value increases from dye **1**–**3**. Unlike for the anionic SDS micelle, binding with TX is largely due to the hydrophobic interactions between the dyes and the micelles since electrostatic interactions are absent. An increase in the K_c value indicates that dye **2** and **3** are more hydrophobic than dye **1**. A similar observation has also been made in CTAB micelles.

We have also measured the fluorescence decay of these dyes in TX. Fig. 5 shows the representative fluorescence decay data of dye **2** in TX. Unlike other media where the fluorescence decay can best be described by a single exponential fit, a double exponential fit is necessary to analyse the decay data in TX. In dye **2** two lifetimes are recorded ($\tau_1 = 1.64$ ns, $\tau_2 = 0.76$ ns). Comparing with the decay data for dye **2** in water, it can be seen that the 1.64 ns lifetime is the same as that for dye **2** in water. This lifetime then corresponds to the single dye molecule fluorescence lifetime. The second lifetime might be the lifetime of the dye–TX complex. In order to get more information for the excited state properties, the concentration effect of the TX has been measured. The fluorescence decay data of dye **2** at different TX concentrations are analyzed globally by linking lifetimes across all decay data and the pre-exponential factors are allowed to float independently. Results are shown in Table 3. Individual χ^2 values for each of the decay data and the global χ^2 values show that the analysis considering two species model is reasonable. Fig. 6 shows the fractions of the two lifetimes changing with the concentration of TX. When the concentration of TX is low, the longer lifetime ($\tau_1 = 1.64$ ns) of the free dye dominates. The fraction of the dye–TX complex lifetime ($\tau_2 = 0.76$ ns) increases with increasing TX concentration. To obtain the decay associated spectra of each species we have also studied the emission wavelength dependence on the fluorescence lifetime at a particular TX concentration and analyzed these decay data globally using the same procedure

Table 3
Global analysis data of dye **2** in TX at different TX concentrations at 25 °C

[TX] (M)	α_1	τ_1 (ns)	α_2	τ_2 (ns)	individual	global χ^2
0	1	1.64	0	0.76	1.18	1.38
3.7×10^{-4}	0.92		0.08		1.28	
7.3×10^{-4}	0.82		0.18		1.32	
1.1×10^{-4}	0.72		0.28		1.27	
3.7×10^{-3}	0.49		0.51		1.24	
6.4×10^{-3}	0.42		0.58		1.37	
9.1×10^{-3}	0.37		0.63		1.12	
1.8×10^{-2}	0.35		0.65		1.40	
2.7×10^{-2}	0.36		0.64		1.30	
3.6×10^{-2}	0.33		0.67		1.26	
4.6×10^{-2}	0.31		0.69		1.28	

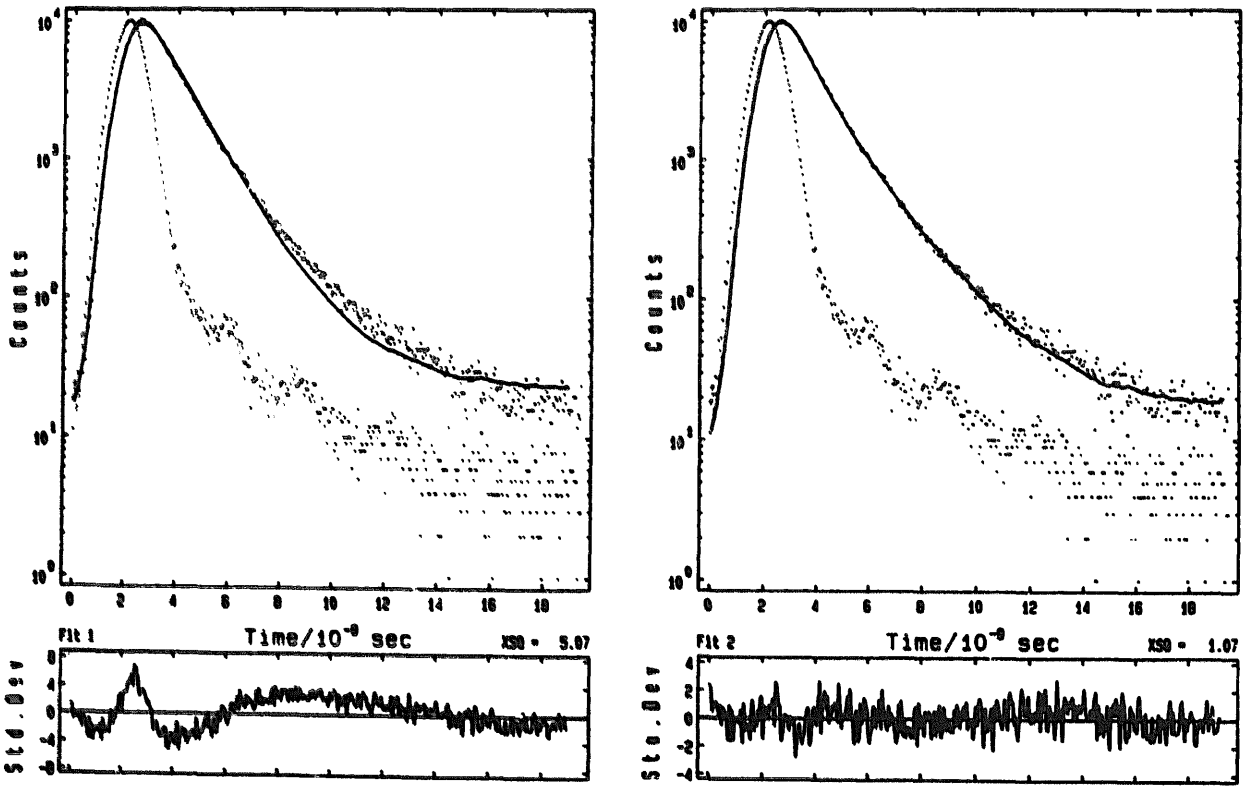

Fig. 5. Typical fluorescence decay curves associated with the lamp profiles for dye **2** in TX. The curves from left to right show the single- and double-exponential fits, residuals and χ^2. Excitation and emission wavelengths are 500 nm and 540 nm respectively. Dye **2** and TX concentrations are 1.8×10^{-6} M and 9.1×10^{-3} M respectively.

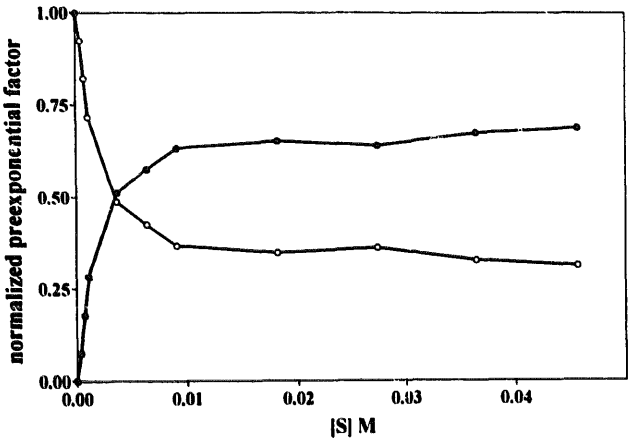

Fig. 6. Influence of TX concentration on normalized pre-exponential factors of the two fluorescence lifetimes of dye 2 (1.8×10^{-6} M) at 25 °C. Excitation and emission wavelengths are 500 nm and 540 nm respectively. (●) represents the 0.76 ns lifetime component and (○) represents the 1.64 ns lifetime component.

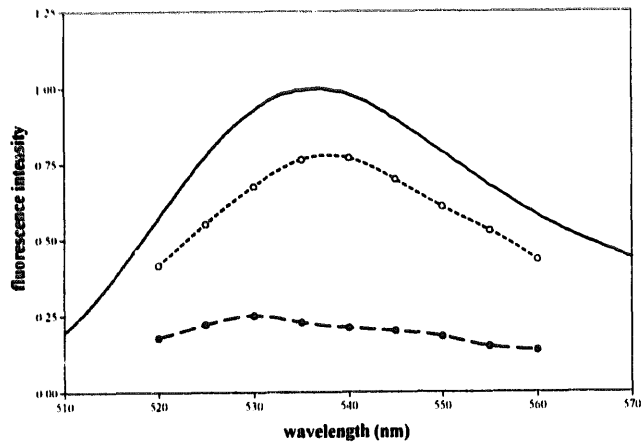

Fig. 7. Steady state fluorescence spectrum (excitation wavelength 480 nm) together with decay associated spectra (DAS) of dye 2 (1.8×10^{-6} M) in TX (1.8×10^{-2} M). (●) represents the 1.64 ns DAS and (○) represents the 0.76 ns DAS. All points in DAS are obtained by global analysis (global $\chi^2 = 1.393$) and lines are cubic spline fittings of these points. Details of analysis are discussed in the text.

as used for the concentration dependence. From the normalized pre-exponential factors we have calculated the fractional contribution to the fluorescence intensity of each-species and subsequently using the steady state emission spectra we recovered the decay associated spectra (DAS) of the individual species. Fig. 7 shows the DAS for dye 2 in TX. From the figure it is clear that the 0.76 ns DAS are red-shifted compared to the 1.64 ns DAS. This again confirms that the shorter lifetime component originates from the dye–TX complexes.

The experimental data presented above are direct spectrophotometric evidence for the molecular interaction between the dyes and the TX surfactant. TX is a non-ionic detergent and consists of a bulky alkyl phenyl group and a long polyoxyethylene (POE) chain that terminated with a hydroxyl (–OH) group. In TX, the cationic dye can penetrate the micelle to form a strong charge-transfer (CT) complex at a polar site [29]. That is the electron rich phenolic group of TX which takes part in the CT interaction with the electron deficient rhodamine dye. However, the long POE chains are polar and thus extend out into the surrounding aqueous environment and the chains are also quite flexible in nature [30–32]. The terminal OH group might also be involved in a hydrogen bonding interaction with the dyes [33]. Comparisons in the quantum yields and the lifetimes of the dyes in TX and in long chain alcohols (Table 1) do favor the first assumption that it is the formation of CT complexes between the dyes and TX. As a consequence of this CT interaction, fluorescence decreases and the decrease is more important for dyes **2** and **3**. Additional channels of non-radiative decay are probably created due to the flexibility of the POE chains. Similar observations like large red shifts in absorption and emission maxima and a decrease in ϕ_F were reported for the cationic phenosafranin [29] and the cresyl violet [33,34] dyes. The hydrophobicity of the dyes also seems to play a role in the complex formation since from Table 2 one can see that the K_c values increase with the molecular volume and the log P values. The hydrophobicity of the dye seems to facilitate its penetration inside the TX micelles.

4. Conclusion

The spectroscopic and photophysical properties of these three cationic dyes in homogeneous solvents indicate that the hydrogen bonding capability of the amino end group lone pair for these dyes increase with the increasing proton donor ability of the solvents.

All these dyes interact with anionic SDS micelles. The interaction is mainly electrostatic in nature. At the low SDS concentration, (below c.m.c.), dye–SDS aggregate formation takes place, but with an increasing SDS concentration progressively dye–SDS disaggregation from the multimer to the monomeric form is induced, and above the c.m.c. homogeneous distribution of the monomeric dye in SDS micelles is obtained. Compared with dyes **1** and **2**, penetration of dye **3** in SDS seems to be lower.

Dye **1** is not soluble in the cationic CTAB micelles. Dyes **2** and **3** show a finite interaction with the CTAB micelles. The hydrophobic interactions are dominant over the coulombic repulsion where in dye **1** coulombic repulsion is the main dominating factor.

All three dyes form strong ground state complexes with neutral TX micelles. As the electrostatic interaction is absent, a complex formation is facilitated by the hydrophobic interaction. The nature of the complex might be a charge–transfer interaction between a phenolic donor group (in TX) and the rhodamine acting as an electron acceptor.

As dyes **2** and **3** are good potential candidates for efficient cancer cell photosensitisers, it is important to know the nature of the dye distribution and the localization inside the cell since the selective biodistribution of an ionic drug in tissues

and membranes depends on its self-interaction properties and the complex interactions with its molecular surroundings. All the spectroscopic and photophysical data of these dyes in homogeneous and microheterogeneous media will be very helpful for a better understanding in the nature of the binding and distribution of these dyes inside living cells. The spectroscopic and photophysical characterization of these dyes in normal and malignant cells is in progress.

Acknowledgment

This work was supported by a grant from the Theratechnologies Inc., Montreal, Qué., Canada and also by grants from NSERC.

References

[1] B.W. Henderson and T.J. Dougherty, *Photochem. Photobiol., 55* (1992) 145.
[2] P. Pal, H. Zeng, G. Durocher, D. Girard, T. Li, A.K. Gupta, R. Giasson, L. Blanchard, L. Gaboury, A. Balassy, C. Turmel, A. Laperrière and L. Villeneuve, *Photochem. Photobiol., 63* (1996) 161.
[3] J.H. Fendler, *Membrane Mimetic Chemistry*, Wiley Interscience, New York, 1982.
[4] M. Duemie and M.E. Baraka, *J. Photochem. Photobiol. A: Chem., 74* (1993) 255.
[5] R.K. Emaus, R. Grunwald and J.J. Lemasters, *Biochim. Biophys. Acta, 850* (1986) 436.
[6] J.M. Millot, S. Sharonov and M. Manfait, *Cytometry, 17* (1994) 50.
[7] K. Kalyanasundaram, in V. Ramamurthy (ed.), *Photochemistry in Organized and Constrained Media*, VCH, New York, 1991.
[8] J.R. Lakowicz, P.A. Koen, H. Szmacinski, I. Gryczysski and J. Kusba, *J. Fluor., 4(1)* (1994) 117.
[9] H. Zeng and G. Durocher, *J. Lumin., 63* (1995) 75.
[10] A. Pradhan, P. Pal, G. Durocher, L. Villeneuve, A. Balassy, F. Babai, L. Gaboury and L. Blanchard, *J. Photochem. Photobiol. B: Biol., 31* (1995) 101.
[11] S. Nigam and G. Durocher, *J. Phys. Chem., 100* (1996) 7135.
[12] J.M. Beechem, *Chem. and Phys. of Lipids, 50* (1989) 237.
[13] L.D. Janssents, N. Boens, M. Ameloot and F.C. De Schryver, *J. Phys. Chem., 94* (1990) 3564.
[14] R.S. Sarpal, M. Belletête and G. Durocher, *J. Phys. Chem., 97* (1993) 5007.
[15] A. Chow, J. Kennedy, R. Pottier and T.G. Truscott, *Photobiochem. Photobiophys., 11* (1986) 139.
[16] B. Zelent, T. Ganguly, L. Farmer, D. Gravel and G. Durocher, *J. Photochem. Photobiol. A: Chem., 56* (1991) 165.
[17] M.J. Snare, F.E. Treloar, K.P. Ghiggino and P.J. Thistlewaite, *J. Photochem., 18* (1982) 335.
[18] *Global Unlimited, Version 1.02-2* (1990), updated in 1993, Laboratory for Fluorescence Dynamics, University of Illinois at Urbana–Champaign.
[19] P. Suppan, *J. Chem. Soc. (A)*, (1968) 3125.
[20] M. Belletête, S. Nigam and G. Durocher, *J. Phys. Chem., 99* (1995) 4015.
[21] M. Belletête, R.S. Sarpal and G. Durocher, *Can. J. Chem., 72* (1994) 2239.
[22] J.H. Fendler and E.J. Fendler, *Catalysis in micellar and macromolecular systems*, Academic Press, New York, 1975.
[23] R.K. Emaus, R. Grunwald and J.J. Lemasters, *Biochim. Biophys. Acta, 850* (1986) 436.
[24] N. Bodor, Z. Gabanyi and C. Wong, *J. Am. Chem. Soc., 111* (1989) 3783.
[25] Hypercube Inc. Scientific Software Waterloo, Ontario, Canada.
[26] M. Belletête, N. Di Cesare, M. Leclerc and G. Durocher, *Chem. Phys. Lett., 250* (1996) 31.
[27] V.N. Viswanathan, A.K. Ghose, G.N. Revankar and R.K. Robbins, *J. Chem. Inf. Comput. Sci., 29* (1989) 163.
[28] H.A. Benesi and J.H. Hildebrand, *J. Am. Chem. Soc., 71* (1949) 2703.
[29] K.K. Rohatgi-Mukherjee, R. Chaudhuri and B.B. Bhowmik, *J. Coll. Interface Sci., 106* (1985) 45.
[30] W.J. Dressick, B.L. Hauenstein Jr., T.B. Gilbert, J.N. Demas and B.A. DeGraff, *J. Phys. Chem., 88* (1984) 3337.
[31] F. Podo, A. Ray and G. Nemethy, *J. Am. Chem. Soc., 95* (1973) 6165.
[32] F.E. Bailey and J.V. Koleske, *Polyethylene oxide)*, Academic Press, New York, 1976.
[33] S.J. Isak and E.M. Eyring, *J. Photochem. Photobiol. A: Chem., 64* (1992) 343.
[34] S.J. Formosinho and M.M. Miguel, *J. Chem. Soc. Faraday Trans. I, 81* (1985) 1891.